Received: Added at production | Revised: Added at production | Accepted: Added at production

DOI: xxx/xxxx

RESEARCH ARTICLE

Mollification of Fourier Spectral Methods with Polynomial Kernels

Megha P | Chandhini G*

[1]Department of Mathematical and Computational Sciences, National Institute of Technology Karnataka, Karnataka, India

Correspondence
*Chandhini G, Department of Mathematical and Computational Sciences, National Institute of Technology Karnataka, Karnataka, India. Email: chandhini@nitk.edu.in

Abstract

Many attempts have been made in the past to regain the spectral accuracy of the spectral methods, which is lost drastically due to the presence of discontinuity. In this article, an attempt has been made to show that mollification using Legendre and Chebyshev polynomial based kernels improves the convergence rate of the Fourier spectral method. Numerical illustrations are provided with examples involving one or more discontinuities and compared with the existing Dirichlet kernel mollifier. Dependence of the efficiency of the polynomial mollifiers on the parameter P is analogous to that in the Dirichlet mollifier, which is detailed by analysing the numerical solution. Further, they are extended to linear scalar conservation law problems.

KEYWORDS:
spectral methods, Gibbs phenomenon, mollifier, Legendre kernel, Chebyshev kernel, linear advection equation

1 | INTRODUCTION

Spectral methods are efficient and robust global numerical methods that provide exponential accuracy while approximating infinitely smooth functions or solutions of differential equations. The spectral accuracy enjoyed by the spectral methods is lost when discontinuous points are present in the domain. Spurious oscillations, known as Gibbs phenomenon, are produced in the solution obtained using these spectral methods. Besides producing the oscillatory solutions, Gibbs phenomenon reduces the spectral accuracy of the method to linear order globally. There are various post-processing techniques to regain the convergence rate of the spectral methods, and mollification is among them. Mollifiers are compactly supported non-negative kernels having unit mass and considered for the convolution with the approximate solution to eliminate Gibbs phenomenon.

In 1985, Gottlieb and Tadmor[1] introduced a mollifier $\psi^{\theta,P}(y) = \theta^{-1}\rho(\theta^{-1}p)D_P(\theta^{-1}y)$. It is the product of a sufficiently smooth cut-off function and the Dirichlet kernel (called regularization kernel). They have proved that convolving the Fourier spectral approximation of a discontinuous function with this regularization kernel recovers the pointwise spectral accuracy depending on the local smoothness of the function. Abarbanel et al.[2] observed that enough information is hidden in the spectral approximation of the discontinuous solution itself. i.e., For any infinitely differentiable function v, $(S_{\mathcal{N}}u(x,t), v(x)) = (u(x,t), v(x)) + \epsilon_1$, where $S_{\mathcal{N}}u(x,t)$ is the Fourier Galerkin approximation of the solution $u(x,t)$ of a linear hyperbolic equation and ϵ_1 is spectrally small. Hence to retrieve spectral accuracy at the points where u is smooth, it is sufficient to find an appropriate function v such that $(u(x,t), v(x)) = u(x,t) + \epsilon_2$, where ϵ_2 is spectrally small. They showed that it is possible to extract accurate pointwise values from $S_{\mathcal{N}}u(x,t)$ using $v \equiv \psi^{\theta,P}$ and the improvements in the accuracy approve their claim.

Close to two decades later, Tadmor and Tanner[3] have modified the above regularization kernel $\psi^{\theta,P}$ as adaptive mollifiers in which the parameters P and θ are optimized according to the number of vanishing moments of the mollifier and discontinuity position, respectively. Convolution with their adaptive mollifier has further improved the accuracy of the Fourier approximation of a piecewise function up to the immediate vicinity of the discontinuous points.The mollifiers discussed thus far are compactly supported. However, Tanner[4] developed a noncompactly supported optimal filter and mollifier for which parameters are chosen

simultaneously for both time and frequency space, thus leading to a more balanced error decomposition. Piotrowska et al.[5], in their recent work, modified the above mollifier to a one-sided, normalized mollifier for each point as given by,

$$\tilde{\Psi}^{d}_{p,N}(x,y) = \begin{cases} \dfrac{\Psi^{d}_{p,N}(x,y)}{\int_{c_j}^{c_{j+1}} \Psi^{d}_{p,N}(x,y)dy} & c_j \le y \le c_j + 1 \\ 0 & otherwise \end{cases} \tag{1}$$

where c_j are jump points, $\Psi^{d}_{p,N}$ is the mollifier defined in[4]. It is shown through examples that they preserve most of the properties of the original discontinuous function considered.

Apart from mollifiers, there are other methods in the literature to mitigate the effects of Gibbs phenomenon and improve the accuracy of the spectral methods. Nira Gruberger[6] introduced new post-processing filters for Fourier and Chebyshev spectral methods by considering corresponding approximations of the Dirac delta function. With a marginal modification of the filter at the point of discontinuity, the results have improved significantly for Burgers' equation but disappointing in the case of astrophysical problem. In 1991, Vandevan[7] has introduced a class of filters that does not require the prior knowledge of the position of the discontinuity and produces exponential accuracy for the filtered solution $\sigma^{u}_{N}(x) = \sum_{k=0}^{N} \sigma(k/N)\hat{u}_k\phi_k(x)$, nevertheless only for points away from the discontinuity. Analogous to the adaptive mollifier, Tadmor constructed an exponential adaptive filter[8], where the parameter p (represents the order of the projection) involved is optimized according to the distance from the discontinuity. The adaptive choice allows the use of lower ordered filter in the close vicinity of the discontinuity and higher order filters for points away from the discontinuity. For Fourier approximation, a Lanczos type filter using sigmoidal function was proposed by Yun and Rim[9], which again provide exponential accuracy for points away from the discontinuity. Kanevsky[10], in their work observed that while solving time-dependent problems, filtering-in-time error become additive for certain numerical methods. To address this, they introduced an idempotent filter, which is also a function of time. Post-processing on spectral method solutions of the nozzle flow problem using these idempotent filters supported their observations.

Another frequently used and well discussed post processing technique is Gegenbauer reconstruction method. In 1992, Gottlieb et al.[11] laid foundation for this idea. Gegenbauer reconstruction method involves projecting the spectral method in a new space of Gegenbauer polynomials. Though the reprojection helped in overcoming Gibbs phenomenon, the method suffers from round-off errors and Runge phenomenon. By incorporating the properties lacked by Gegenbaur polynomials, a robust Gibbs complementary basis was introduced[12]. In this work, they proposed to use Freud polynomials over the Gegenbauer polynomials for the reprojection space, despite not having concrete theory on the optimum Gibbs complementary basis. Recently, Chen and Shu[13] have analysed linear transport problems having initial conditions with singular derivatives using Gegenbaur reconstruction and Faghihifar and Akbari[14] proved the robustness of Gegenbaur reconstruction method against truncated convolution error. An inverse polynomial reconstruction method, inspired from Gegenbauer reconstruction method, was proposed by Shizgal and Jung[15] and the betterment happend over the years[16].

Eckhoff[17] developed a reconstruction method in which a discontinuous function with M number of jumps is reconstructed as a linear combination of step function and a continuous function. Eckhoff's algorithm also determines the jumps and the location of discontinuity. Some modifications on this algorithm in terms of identifying the jump positions and improving the accuracy can be found in the literature[18,19]. Driscoll and Fornberg[20] introduced a singular Fourier–Padé approximation method and a superior accuracy even at the point of discontinuity was obtained. An extension of Fourier Padé approximation using both Galerkin and collocation approaches[21] for Boussinesq convection flow was also studied. In a later work[22] and the references therein, Padé approximation in terms of orthogonal polynomials can be found. Spectral viscosity and essentialy non-oscillatory techniques are the other approaches commonly considered to handle shock/discontinuity while solving nonlinear conservation law model problems. Based on Fourier basis, Tadmor[23] introduced a spectral vanishing viscosity method, which recovers spectral convergence properties by adding a convolution kernel to the artifical viscosity term to control the dissipation. This also helped the scheme to be stable especially for nonlinear problems. Some of the later works discuss further improvements on spectral viscocity approach in the context of spectral methods and their extension to nonlinear problems[24,25,26,27]. In 2021, a feedforward multiperceptron artificial neural network has been used to predict the regularity of the solution that helps in tuning many parameters in artificial viscocity term added to suppress oscillations[28]. An essentially non-oscillatory spectral method was proposed by Wei Cai et al.[29] in which a saw-tooth function is added to the Fourier basis functions. Similarly, in a more recent work[30], Gibbs oscillation was suppressed by adding Fourier coefficient of suitable Heaviside functions to that of the discontinuous function and uniform convergence was proved.

From the literature on spectral mollifiers[1,3], it is clear that we need a kernel function υ such that the regularization error should be spectrally small. i.e., The difference between $(u(x), \upsilon(x))$ and $u(x)$ is spectrally small. The Dirichlet kernel is one kernel

among them, which is also a spectral approximation of the delta function. Gottlieb et al.[1] used this idea to recover the accuracy of the Fourier spectral method when applied to problems having discontinuous solutions. In an earlier report in 1984[31] and above article[1], they have proposed mollifiers based on Legendre and Chebyshev kernels for Legendre and Chebyshev spectral methods, respectively. Later in 1994, Kaber[32] gave a detailed convergence analysis of mollification by Legendre polynomial kernels on Legendre spectral methods.

The results given in the present article have been motivated by the ideas discussed by Gottlieb and Tadmor[1] and Kaber[32]. In their work, Legendre and Chebyshev spectral approximations were mollified by Legendre and Chebyshev polynomial based kernels, respectively. In our work, we have proposed Legendre and Chebyshev polynomial mollifiers to Fourier spectral method. These mollifiers are an alternative approach to the Dirichlet mollifier proposed by Gottlieb and Tadmor[1]. Convergence analysis shows that the spectral accuracy of the Fourier approximation has been regained with these Legendre and Chebyshev polynomial mollifiers, nevertheless at the points away from the discontinuity. Convergence results have been extensively verified by applying it to Fourier approximation of the one and two-dimensional functions having discontinuities and to the Fourier-Galerkin solution of linear PDEs with discontinuous initial data. Further, polynomial mollified Fourier approximate solutions are compared with the corresponding Dirichlet mollified Fourier approximations[1,3]. It is observed that different choices of the parameter P in each sub-interval have continuously improved the accuracy and considerably reduced the length of the "low accurate" region in the vicinity of the discontinuity. This shows that there is scope for improving the present work by optimizing the parameter P.

In Section 2, some of the preliminary definitions and results have been provided. Recovery of the spectral accuracy of the Fourier approximation using polynomial mollifiers has been detailed in section 3. Section 4 provides various examples to show the efficacy and possible limitations.

2 | PRELIMINARIES

The truncated Fourier series of a 2π periodic function u is,

$$S_{\mathcal{N}}u(x) = \sum_{|k|\leq N} \hat{u}_k e^{ikx} = D_N * u(x), \tag{2}$$

where, D_N is the Dirichlet kernel, $D_N = \dfrac{1}{2\pi}\displaystyle\sum_{|k|\leq N} e^{ikx}$.

The convergence rate of spectral methods depends upon the differentiability of the function u. The following theorem discuss about the spectral convergence of the Fourier spectral method[33].

Theorem 1. If a function $u(x)$, its first $(s-1)$ derivatives and their periodic extensions are all continuous and if the s^{th} derivative $u^{(s)}(x) \in L^2([-\pi,\pi])$, then $\forall\ k \neq 0$ the Fourier coefficients, $\hat{u}_k$, of $u(x)$ decay as $|\hat{u}_k| \propto (\frac{1}{k})^s$. □

Hence, an exponential convergence rate is obtained if the function is infinitely smooth. When discontinuity or non-smoothness is present in the method, it drastically spoils spectral convergence all over the domain.
Define the weighted Sobolev space,

$$H^s_\omega([-\pi,\pi]) = \{u \in L^2_\omega([-\pi,\pi]) : \frac{d^i}{dx^i}u \in L^2_\omega([-\pi,\pi]),\ \forall i\ \ 0 \leq i \leq s\}$$

The convergence results of Fourier spectral method is discussed in detail in terms of Sobolev norm by Canuto et al.[34]. i.e., for $u \in H^s_p([-\pi,\pi])$,

$$\|u - S_N u\|_{L^2([-\pi,\pi])} \leq c_s N^{-s} \|u^{(s)}\|_{L^2([-\pi,\pi])} \leq c_s N^{-s} \|u\|_{H^s([-\pi,\pi])} \quad s \geq 1, \tag{3}$$

where p denotes the periodicity and c_s is a generic constant.

Polynomial spectral methods include representing a function as truncated series with orthogonal polynomials. Legendre, Chebyshev, Hermite, Laguerre spectral methods are some of the well-known polynomial spectral methods. They also give spectral accuracy when the approximating function is infinitely smooth. To overcome the Gibbs phenomenon due to discontinuties, one choice is to construct a mollifier that could approximate Dirac delta function spectrally. Hence we consider suitable mollifiers based on Legendre and Chebyshev polynomials[1].

The Legendre spectral method is defined as,

$$\Pi_N u(x) = \sum_{k=0}^{N} u_k^* L_k(x),$$

where, $u_k^* = \int_{-1}^{1} \frac{u(y)L_k(y)dy}{\|L_k\|^2}$ and L_k is the Legendre polynomial of degree k. The following equation shows the relation between the spectral accuracy of the Legendre spectral method and the smoothness of a function[34]. If $u \in H^s([-1,1])$,

$$|\Pi_N u(x) - u(x)| \leq c_s N^{\frac{3}{4}-s} \|u\|_{H^s([-1,1])} \tag{4}$$

Similarly, the Chebyshev spectral method is defined as,

$$\Pi_N^1 u(x) = \sum_{k=0}^{N} u_k^* T_k(x),$$

where, $u_k^* = \int_{-1}^{1} \frac{u(y)T_k(y)}{\|T_k\|^2} \frac{1}{\sqrt{1-y^2}} dy$ and T_k is the Chebyshev polynomial of degree k.

The spectral convergence of the Chebyshev spectral method is given by the following result[34]. If $u \in H_\omega^s([-1,1]$,

$$|\Pi_N^1 u(x) - u(x)| \leq c_s \log N N^{-s} \|u\|_{s,\infty}, \tag{5}$$

where $\|u\|_{s,\infty} = \max_{0\leq k\leq s} \|u^{(k)}\|_\infty$ and $\omega(y) = \frac{1}{\sqrt{1-y^2}}$.

Inverse inequality of algebraic polynomial[34] is used in the next section. For an algebraic polynomial $q(x)$ with degree n,

$$\|q^{(m)}\|_{L_\omega^p([-1,1])} \leq Cn^{2m} \|q\|_{L_\omega^p([-1,1])}, \quad 2 \leq p \leq \infty. \tag{6}$$

The following section describes how polynomial based kernels can be used in Fourier spectral method as a mollifier to improve accuracy.

3 | MOLLIFICATION IN FOURIER SPECTRAL METHODS USING POLYNOMIAL KERNELS

Mollification is one among many methods used to regain the accuracy of the spectral methods which is lost due to the presence of the discontinuities.

Definition 1. The process, mollification, is convolving the approximation with a unit mass, which is compactly supported non-negative kernel Ψ. i.e.,

$$\mathcal{S}_{\mathcal{N}} u * \Psi(x) = \int_{-\pi}^{\pi} \mathcal{S}_{\mathcal{N}} u(x)\Psi(x-y)dy.$$

The function Ψ is called mollifier. The corresponding action in Fourier space is called filtering, which is defined by

$$\mathcal{S}_{\mathcal{N}}{}^{\sigma} u(x) = \sum_{k=0}^{N} \sigma(k/N)\hat{u}_k e^{ikx}$$

where σ is called filter. It is a $C^\infty([-\pi,\pi])$ even function, whose support is $[-\pi,\pi]$ and $\sigma(0) = 1$.

To obtain the mollifier, we consider the function ρ, a C^∞ function that vanishes outside the given interval. In the present work we consider, $\rho : \mathbb{R} \to \mathbb{R}$, as,

$$\rho(\zeta) = \begin{cases} e^{\frac{\alpha\zeta^2}{\zeta^2-1}}, & \zeta \in (-1,1) \\ 0, & \zeta \notin (-1,1),\ \alpha \text{ is a constant.} \end{cases} \tag{7}$$

3.1 | Legendre polynomial based mollifier

Define the kernel, $K_P : [-1,1] \to \mathbb{R}$,

$$\begin{aligned} K_p(\zeta) &= \sum_{k=0}^{P} \frac{L_k(\zeta)L_k(0)}{\|L_k\|^2}, \\ &= \frac{P+1}{2}\frac{L_{P+1}(\zeta)L_P(0) - L_{P+1}(0)L_P(\zeta)}{\zeta} \end{aligned} \tag{8}$$

Also define the mollifier,

$$\psi^{\theta,P}(x) = \frac{1}{\pi\theta}\rho\left(\frac{x}{\pi\theta}\right)K_P\left(\frac{x}{\pi\theta}\right), \quad x \in [-\pi,\pi]. \tag{9}$$

The parameter θ is defined in such a way that, it is the distance between the point x and the nearest discontinuity point of the function given u.

$$\theta = \frac{1}{\pi} dist(x, \text{discontinuity point of } u). \tag{10}$$

Applying the mollification on the truncated Fourier series $S_N u$ by defining, [1]

$$(S_N u * \psi^{\theta,P})(x) = \int_{-\pi}^{\pi} (S_N u)(y)\psi^{\theta,P}(y-x)dy. \tag{11}$$

Then the total error is decomposed as,

$$(S_N u * \psi^{\theta,P})(x) - u(x) = (S_N u - u) * S_N\psi^{\theta,P}(x) + (S_N u - u) * (\psi^{\theta,P} - S_N\psi^{\theta,P})(x) + (u * \psi^{\theta,P} - u)(x). \tag{12}$$

Considering the first term,

$$(S_N u - u) * S_N\psi^{\theta,P}(x) = \left(\sum_{|k|\le N} \hat{u}_k e^{ikx} - u(y), \sum_{|j|\le N} \hat{\psi}_j e^{ij(y-x)}\right). \tag{13}$$

For a particular 'j,'

$$\begin{aligned} \left(\sum_{|k|\le N} \hat{u}_k e^{ikx} - u(y), \hat{\psi}_j e^{ij(y-x)}\right) &= \left(\sum_{|k|\le N} \hat{u}_k e^{ikx}, \hat{\psi}_j e^{ij(y-x)}\right) - \left(u(y), \hat{\psi}_j e^{ij(y-x)}\right) \\ &= \overline{\hat{\psi}}_j e^{ijx}\hat{u}_j\left(e^{ijy}, e^{ijy}\right) - \overline{\hat{\psi}}_j e^{ijx}\hat{u}_j\left(e^{ijy}, e^{ijy}\right) \\ &= 0. \end{aligned}$$

Thus (13) becomes,

$$(S_N u - u) * S_N\psi^{\theta,P}(x) = 0. \tag{14}$$

Now the two terms remaining in the total error (12) is referred as truncation error and regularization error respectively.

$$\begin{aligned} (S_N u * \psi^{\theta,P})(x) - u(x) &= (S_N u - u) * (\psi^{\theta,P} - S_N\psi^{\theta,P}) + (u * \psi^{\theta,P} - u) \\ &= T_N^{\theta,P}u(x) + R_N^{\theta,P}u(x). \end{aligned} \tag{15}$$

In the following, we prove the spectral accuracy of the truncation and regularization error in (15).

Lemma 1. If $u \in H_p^s([-\pi,\pi])$, then the truncation error satisfies,

$$|T_N^{\theta,P}u(x)| \le c_s N^{-(s+m)}\|\psi^{\theta,P}\|_{H^m([-\pi,\pi])}\|u\|_{H^s([-\pi,\pi])}, \quad m, s \ge 1. \tag{16}$$

Where c_s is a constant.

[1] In equation 11 we are not using the usual definition of convolution, instead we define it as, $(f * g)(x) = \int_\Omega f(y)g(y-x)dy$

Proof.

$$\begin{aligned}
|T_N^{\theta,P}u(x)| &= |(S_N u - u) * (\psi^{\theta,P} - S_N\psi^{\theta,P})(x)| \\
&\leq \int_{-\pi}^{\pi} |(S_N u - u)(y)(\psi^{\theta,P} - S_N\psi^{\theta,P})(y-x)dy| \\
&\leq \|\psi^{\theta,P} - S_N\psi^{\theta,P}\|_{L^2([-\pi,\pi])}\|(S_N u - u)\|_{L^2([-\pi,\pi]),} \\
&\leq c_s N^{-(s+m)}\|\psi^{\theta,P}\|_{H^m([-\pi,\pi])}\|u\|_{H^s([-\pi,\pi]),} \qquad \because by\ (3).
\end{aligned}$$

□

Lemma 2. If $u \in H^s([-\pi,\pi])$, then the regularization error satisfies,

$$|R_N^{\theta,P}u(x)| \leq c_s P^{\frac{3}{4}-s}\|\phi^{\theta,x}\|_{H^s([-1,1])},\ s \geq 1. \tag{17}$$

Where c_s is a constant and $\phi^{\theta,x}(\zeta) = u(x+\theta\pi\zeta)\rho(\zeta) - u(x)$.

Proof.

$$\begin{aligned}
|R_N^{\theta,P}u(x)| &= \left|\int_{-\pi}^{\pi} u(y)\psi^{\theta,P}(y-x)dy - u(x)\right| \\
&= \left|\int_{-\pi}^{\pi} u(y)\frac{1}{\pi\theta}\rho\left(\frac{y-x}{\pi\theta}\right)K_p\left(\frac{y-x}{\pi\theta}\right)dy - u(x)\right| \\
&= \left|\int_{x-\pi\theta}^{x+\pi\theta} u(y)\frac{1}{\pi\theta}\rho\left(\frac{y-x}{\pi\theta}\right)K_p\left(\frac{y-x}{\pi\theta}\right)dy - u(x)\right|.
\end{aligned}$$

Let, $\frac{y-x}{\pi\theta} = \zeta \Rightarrow y = x + \theta\pi\zeta$.

$$|R_N^{\theta,P}u(x)| = \left|\int_{-1}^{1}(u(x+\theta\pi\zeta)\rho(\zeta) - u(x))K_P(\zeta)d\zeta\right| \tag{18}$$

$$= \left|\int_{-1}^{1}\phi^{\theta,x}(\zeta)K_P(\zeta)d\zeta\right| \tag{19}$$

For any function $f \in H_s([-1,1])$,

$$\int_{-1}^{1} f(y)K_P(y)dy = \int_{1}^{1} f(y)\sum_{k=0}^{P}\frac{L_k(y)L_k(0)dy}{\|L_k\|^2} = \sum_{k=0}^{P}L_k(0)\int_{-1}^{1} f(y)\frac{L_k(y)dy}{\|L_k\|^2} = \sum_{k=0}^{P} f_k^* L_k(0) = \Pi_P f(0).$$

Hence,

$$|R_N^{\theta,P}u(x)| = \left|\Pi_P\phi^{\theta,x}(0)\right| \tag{20}$$

Using the spectral accuracy of the Legendre spectral method as given in Equation (4), Equation (20) becomes,

$$|R_N^{\theta,P}u(x)| = |\Pi_P\phi^{\theta,x}(0) - \phi^{\theta,x}(0)| \leq c_s P^{\frac{3}{4}-s}\|\phi^{\theta,x}\|_{H^s([-1,1]),} \quad \because \phi^{\theta,x}(0) = 0.$$

□

To further simplify truncation and regularization errors, consider the following lemma.

Lemma 3. Following estimate holds for the regularization kernel $\psi^{\theta,P}$.

$$\left\|\psi^{\theta,P}(x)\right\|_{H^m([-\pi,\pi])} \leq c_m \frac{1}{\theta} P^2 \left(\frac{P^2}{\theta^2}+\frac{1}{\theta}\right)^m \|\rho\|_m \tag{21}$$

$$where,\ \|\rho\|_m^2 = \sum_{l=0}^{m}\sum_{j=0}^{l}\int_{-\pi}^{\pi}\binom{l}{j}\left|\rho^{(j)}\left(\frac{x}{\theta\pi}\right)\right|^2 dx, \qquad m \geq 1.$$

Proof.

$$For\ \ l \leq m,\ \ \left|\frac{d^l}{dx^l}\psi^{\theta,P}(x)\right| = \left|\sum_{j=0}^{l}\binom{l}{j}\frac{1}{\theta\pi}\rho^{(j)}\left(\frac{x}{\theta\pi}\right)\frac{1}{(\theta\pi)^l}K_P^{(l-j)}\left(\frac{x}{\theta\pi}\right)\right| \tag{22}$$

Using, (6) and the fact that $\|L_k\|^2 = \dfrac{2}{2k+1}$, we can show that,

$$\begin{aligned}\left|K_P^{(l-j)}\left(\frac{x}{\theta\pi}\right)\right| &\leq \frac{1}{(\theta\pi)^{l-j}}\sum_{k=0}^{P}\frac{\left|L_k^{(l-j)}\left(\frac{x}{\theta\pi}\right)L_k(0)\right|}{\|L_k\|^2}\\ &\leq \frac{c}{\theta^{l-j}}P^2P^{2(l-j)},\quad c\ is\ a\ constant.\end{aligned}$$

Substituting (23) in (22)

$$\left|\frac{d^l}{dx^l}\psi^{\theta,P}(x)\right| \leq c\sum_{j=0}^{l}\binom{l}{j}\frac{\theta^j}{\theta^{2l+1}}\left|\rho^{(j)}\left(\frac{x}{\theta\pi}\right)\right|P^2P^{2(l-j)} \tag{23}$$

Applying the Cauchy-Schwarz inequality,

$$\begin{aligned}\left|\frac{d^l}{dx^l}\psi^{\theta,P}(x)\right|^2 &\leq c\frac{1}{\theta^{4l+2}}\sum_{j=0}^{l}\binom{l}{j}\left|\rho^{(j)}\left(\frac{x}{\theta\pi}\right)\right|^2\sum_{j=0}^{l}\binom{l}{j}\theta^{2j}\left(P^2P^{2(l-j)}\right)^2 \qquad (24)\\ &\leq c\frac{P^4}{\theta^2}\left(\frac{P^4}{\theta^4}+\frac{1}{\theta^2}\right)^l\sum_{j=0}^{l}\binom{l}{j}\left|\rho^{(j)}\left(\frac{x}{\theta\pi}\right)\right|^2\end{aligned}$$

$$\sum_{l=0}^{m}\int_{-\pi}^{\pi}\left|\frac{d^s}{dx^s}\psi^{\theta,P}(x)\right|^2 dx \leq c_m\frac{P^4}{\theta^2}\left(\frac{P^4}{\theta^4}+\frac{1}{\theta^2}\right)^m\sum_{l=0}^{m}\sum_{j=0}^{l}\int_{-\pi}^{\pi}\binom{l}{j}\left|\rho^{(j)}\left(\frac{x}{\theta\pi}\right)\right|^2 dx$$

$$Hence,\quad \left\|\frac{d^m}{dx^m}\psi^{\theta,P}(x)\right\|_{H^m([-\pi,\pi])} \leq c_m\frac{1}{\theta}P^2\left(\frac{P^2}{\theta^2}+\frac{1}{\theta}\right)^m\|\rho\|_m.$$

□

Lemma 4.

$$\|\phi^{\theta,x}\|_{H^s([-1\ 1])} \leq c_s\left(1+\theta^2\right)^{s/2}\max_{\substack{0\leq k\leq s\\ |x-y|\leq\pi\theta}}|D^{(k)}u(y)\|\rho\|_s,\quad s \geq 1. \tag{25}$$

Proof.

$$For \quad l \le s, \quad \left|\frac{d^l}{d\zeta^l}\phi^{\theta,x}(\zeta)\right| \le \sum_{j=0}^{l}\binom{l}{j}\left|(D^{(l-j)}u)(x+\theta\pi\zeta)(\theta\pi)^{l-j}\rho^{(j)}(\zeta)\right|$$

$$\le (\theta\pi)^l \max_{\substack{0\le k\le s\\ |x-y|\le\pi\theta}}|D^{(k)}u(y)| \sum_{j=0}^{l}\binom{l}{j}\frac{1}{(\theta\pi)^j}\left|\rho^{(j)}(\zeta)\right|$$

$$\left|\frac{d^l}{d\zeta^l}\phi^{\theta,x}(\zeta)\right|^2 \le (\theta\pi)^{2l}\left(\max_{\substack{0\le k\le s\\ |x-y|\le\pi\theta}}|D^{(k)}u(y)|\right)^2 \sum_{j=0}^{l}\binom{l}{j}\frac{1}{(\theta\pi)^{2j}}\sum_{j=0}^{l}\binom{l}{j}\left|\rho^{(j)}(\zeta)\right|^2$$

$$\le (\theta\pi)^{2l}\left(1+\frac{1}{(\theta\pi)^2}\right)^l\left(\max_{\substack{0\le k\le s\\ |x-y|\le\pi\theta}}|D^{(k)}u(y)|\right)^2\sum_{j=0}^{l}\binom{l}{j}\left|\rho^{(j)}(\zeta)\right|^2$$

$$\sum_{l=0}^{s}\int_{-\pi}^{\pi}\left|\frac{d^l}{d\zeta^l}\phi^{\theta,x}(y)\right|^2 d\zeta \le (\theta\pi)^{2s}\left(1+\frac{1}{(\theta\pi)^2}\right)^s\left(\max_{\substack{0\le k\le s\\ |x-y|\le\pi\theta}}|D^{(k)}u(y)|\right)^2\sum_{l=0}^{s}\int_{-\pi}^{\pi}\sum_{j=0}^{l}\binom{l}{j}\left|\rho^{(j)}(\zeta)\right|^2 d\zeta.$$

Thus,

$$\|\phi^{\theta,x}\|_{H^s([-1\ 1])} \le c_s\left(1+\theta^2\right)^{s/2}\max_{\substack{0\le k\le s\\ |x-y|\le\pi\theta}}|D^{(k)}u(y)|\|\rho\|_s.$$

□

Now, we state the main theorem of our approach, which is a combined result of Lemma 1 to Lemma 4.

Theorem 2. Let $u \in H_p^s([-\pi,\pi])$. The Fourier spectral approximation of u is $S_N u$, and $\psi^{\theta,P}$ is defined as in the equation (9). Then,

$$\left|S_N u * \psi^{\theta,P}(x) - u(x)\right| \le c_s\left(\|\rho\|_m N^{-(s+m)}\frac{P^2}{\theta}\left(\frac{P^2}{\theta^2}+\frac{1}{\theta}\right)^m\|u\|_{H^s([-\pi,\pi])}\right.$$
$$\left. + \|\rho\|_s P^{\frac{3}{4}-s}\left(1+\theta^2\right)^{s/2}\max_{\substack{0\le k\le s\\ |x-y|\le\pi\theta}}|D^{(k)}u(y)|\right) \quad (26)$$

Remark 1. The equation (26) shows the spectral accuracy of the method. The accuracy of the method increases when the smoothness of the function increases. If $s = m$ and $P = N^{1/2}$, then truncation error is of order $O(N^{-s+1})$ and regularization error is of order $O(N^{3/8-s/2})$.

3.2 | Chebyshev polynomial based mollifier

Define, $K_p : [-1\ 1] \to \mathbb{R}$,

$$K_p(\zeta) = \sum_{k=0}^{P}\frac{T_k(\zeta)T_k(0)}{\|T_k\|^2}. \quad (27)$$

where T_k is the Chebyshev polynomial of degree k. Then, the kernel $\psi^{\theta,P}$ can be defined as given in the equation (9). All the results obtained for Legendre polynomial based mollifier could be proved also for Chebyshev polynomial based kernel. The main theorem can be stated as follows.

Theorem 3. Let $u \in H_p^s([-\pi,\pi])$. The Fourier spectral approximation of u is $S_N u$, and $\psi^{\theta,P}$ is defined as in the equation (9). Then,

$$\left|S_N u * \psi^{\theta,P}(x) - u(x)\right| \leq c_s \left(\|\rho\|_m N^{-(s+m)} \frac{P}{\theta}\left(\frac{P^2}{\theta^2} + \frac{1}{\theta}\right)^m \|u\|_{H^s([-\pi,\pi])} + \|\rho_1\|_{s,\infty} \log P P^{-s} (1+\theta)^s \max_{\substack{0\leq k\leq s \\ |x-y|\leq \pi\theta}} |D^{(k)}u(y)| \right), \quad (28)$$

where $\rho_1(\zeta) = \rho(\zeta)\sqrt{1-\zeta^2}$.

In the next section, recovery of the spectral accuracy of Fourier approximation proved in the Theorem 2 and Theorem 3 is illustrated through various examples having discontinuities.

4 | NUMERICAL EXAMPLES

In this section, mollified solutions have been compared in detail for examples involving discontinuities. Further, mollification is applied to the Fourier-Galerkin solution of the linear scalar conservation law equation with discontinuous initial conditions.

For Legendre and Chebyshev polynomial mollifiers, we have mollified the solutions using constant P and varying P in different parts of the sub-domain. Values of P are chosen by trial and error approach. In their numerical experiments using Dirichlet kernel mollifier, Gottlieb et al.[1] have also observed that better results are obtained when $P = N^{0.8}$. Hence we have chosen the same parameters for the Dirichlet mollifier to compare our results in one dimension. However, for the given two-dimensional example, $N^{0.8}$ does not provide optimum accuracy.

4.1 | Mollification on Fourier approximation of functions

Consider Example 1, where the function is discontinuous at a single point $x = \pi$. The Fourier spectral approximation of this function with the number of terms $N = 64$ is mollified using Legendre and Chebyshev polynomial mollifiers and compared with the Dirichlet mollifier.

Example 1.

$$u(x) = \begin{cases} x, 0 \leq x \leq \pi \\ x - 2\pi, \pi < x \leq 2\pi. \end{cases}$$

Figure 1(a) is the graph of the exact function, Fourier approximation, and mollified Fourier approximations using Legendre, Chebyshev, and Dirichlet mollifiers. Even after mollification, the Gibbs oscillation is not getting damped out at the close vicinity of the discontinuity. Figure 1(b) shows that the mollified solutions at the boundaries using Legendre and Chebyshev kernels are marginally better when compared with the Dirichlet mollified solution. The neighbourhood region, where the accuracy is lost due to discontinuity is marginally smaller for polynomial kernels compared to Dirichlet one. Table 1 shows the error of the solution at some points in the domain. It is clear that the error has reduced significantly for all the kernels for the points away from the discontinuity.

The Dirichlet mollifier introduced by Gottlieb and Tadmor[1] was modified by Tadmor and Tanner[3] in 2002. They optimized the parameter P involved in the mollifier so that it depends on the distance between the discontinuous and the evaluation points. By choosing P adaptively, they could improve the results in[1] and up to the close vicinity of the discontinuity.

From equation (26) and through our numerical experiments, we have observed that the error depends upon the parameter P of the mollifier. For Example 1, we have also mollified the Fourier approximation by choosing different P in two sub-intervals in the case of polynomial mollifiers. At the points away from the discontinuity, we have chosen $P = N$, and near the discontinuity, $P = N/2$. The Figures 1(c) and 1(d) give the error graphs where the results are compared with the Dirichlet mollifier with $P = N^{0.8}$ and adaptive P given in the literature[1,3].

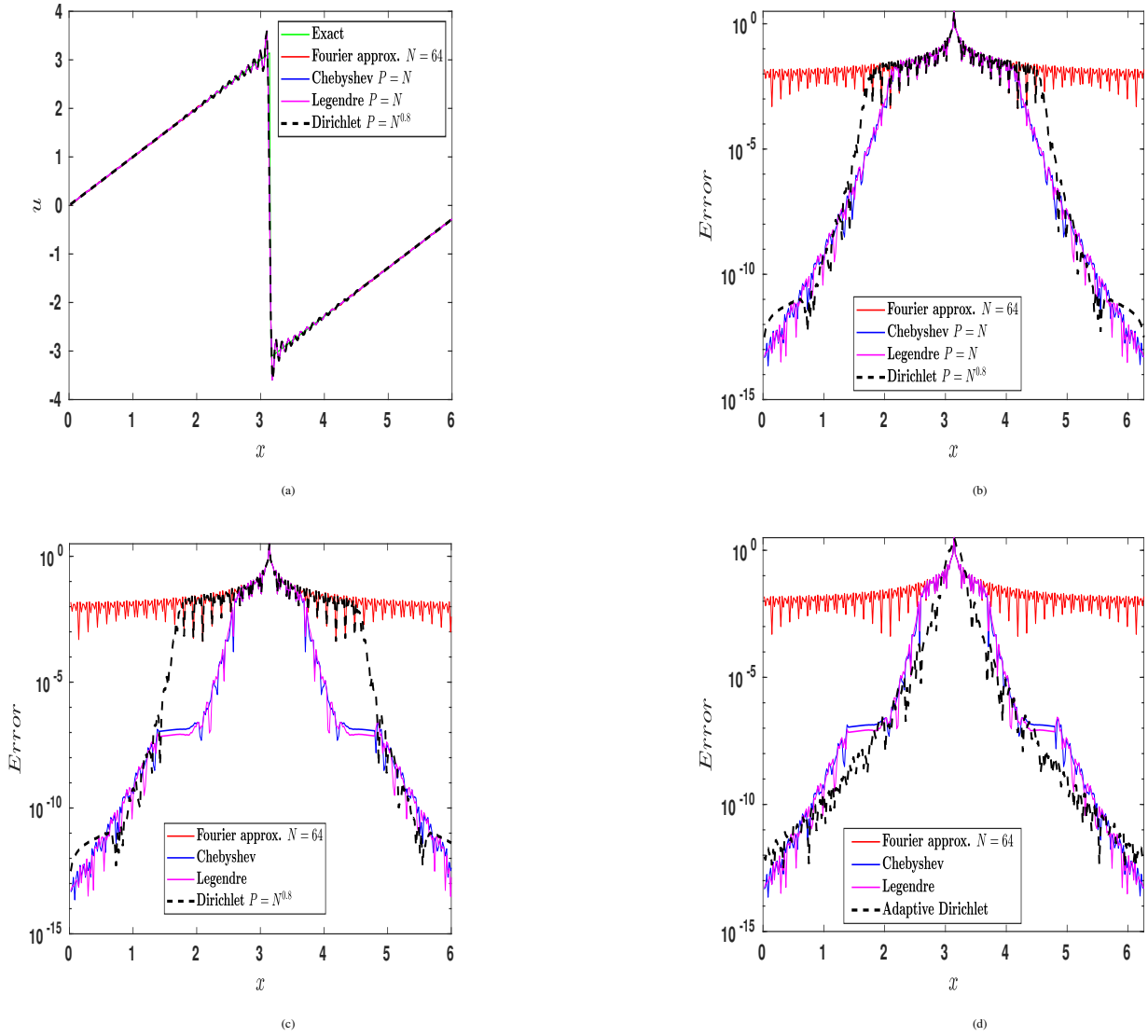

Figure 1 Example 1:-Plots of, (a) solution graphs - exact, unmollified and mollified using Legendre, Chebyshev and Dirichlet kernels. (b) Corresponding pointwise error graphs. (c) Legendre and Chebyshev mollification using different P values in different parts of the domain, Dirichlet remain same as in (b), (d) Legendre and Chebyshev mollification is same as in (c), Adaptive Dirichlet mollification by Tadmor and Tanner[3].

The errors plotted in Figures 1(c) and 1(d) and given in Table 2 show that the interval where the accuracy is lost in the neighborhood of the discontinuity has contracted significantly when different P is used for polynomial mollifiers. This improvement could also be observed through the errors at $x = 1.9059, 2.0944, 4.1888, 4.5029$ in Tables 1 and 2.

In the next example, we consider a function having discontinuities at an interior point as well as at the boundaries.

Example 2.

$$u(x) = \begin{cases} (2e^{2x} - 1 - e^{\pi})/(e^{\pi} - 1), & 0 \le x < \pi/2 \\ -\sin(2x/3 - \pi/3), & \pi/2 \le x < 2\pi. \end{cases}$$

It is a function having discontinuous points $0, \pi/2$ and 2π. Similar behavior as in Example 1 is observed in this example too. Figures 2(a) and 2(b) give solution and error graphs of unmollified and mollified approximations. Results in Figure 2(b) and Table 3 show that polynomial mollifiers have a slightly smaller window of high errors near the discontinuity $\pi/2$, when

Table 1 Absolute error using Dirichlet, Legendre, Chebyshev kernel mollified solution of Example 1. The discontinuity point is π.

Points	Unmollified	Dirichlet [1]	Legendre	Chebyshev
0.0419	0.0066	6.2×10^{-13}	7.5×10^{-14}	5.7×10^{-14}
0.1047	0.0070	1.5×10^{-12}	1.4×10^{-13}	1.7×10^{-13}
0.2094	0.0126	3.1×10^{-12}	5.4×10^{-13}	3.3×10^{-13}
0.6283	0.0050	9.4×10^{-12}	7.7×10^{-12}	1.4×10^{-12}
1.0472	0.0179	1.1×10^{-9}	1.5×10^{-9}	2.5×10^{-9}
1.9059	0.0109	0.0110	0.0002	0.0002
2.0944	0.0004	0.0004	0.0026	0.0025
2.6180	0.0411	0.0411	0.0411	0.0411
3.1206	0.6992	0.6992	0.6992	0.6992
3.1625	0.6992	0.6992	0.6992	0.6992
4.1888	0.0004	0.0004	0.0026	0.0025
4.5029	0.0243	0.0145	1.8×10^{-5}	2.7×10^{-5}
5.2360	0.0179	1.1×10^{-9}	1.5×10^{-9}	2.5×10^{-9}
5.6549	0.0050	9.4×10^{-12}	7.7×10^{-12}	1.4×10^{-13}
6.2413	0.0066	6.1×10^{-13}	7.2×10^{-14}	5.4×10^{-14}

Table 2 Absolute error using Dirichlet, adaptive Dirichlet, Legendre, Chebyshev kernel mollified solution of Example 1. The discontinuity point is π.

Points	Unmollified	Dirichlet [1]	Adaptive Dirichlet [3]	Legendre (different P)	Chebyshev (different P)
0.0419	0.0066	6.2×10^{-13}	6.5×10^{-13}	7.5×10^{-14}	5.7×10^{-14}
0.1047	0.0070	1.5×10^{-12}	1.0×10^{-12}	1.4×10^{-13}	1.7×10^{-13}
0.2094	0.0126	3.1×10^{-12}	4.0×10^{-12}	5.4×10^{-13}	3.3×10^{-13}
0.6283	0.0050	9.4×10^{-12}	8.8×10^{-12}	7.7×10^{-12}	1.4×10^{-11}
1.0472	0.0179	1.1×10^{-9}	1.5×10^{-10}	1.5×10^{-9}	2.5×10^{-9}
1.9059	0.0109	0.0110	1.8×10^{-7}	9.8×10^{-8}	1.7×10^{-7}
2.0943	0.0004	0.0004	6.7×10^{-8}	1.8×10^{-7}	2.1×10^{-7}
2.6180	0.0410	0.0411	0.0001	0.0166	0.0148
3.1206	0.6992	0.6992	2.1854	0.6992	0.6992
3.1625	0.6992	0.6992	2.1854	0.6992	0.6992
4.1888	0.0004	0.0004	6.7×10^{-8}	1.8×10^{-7}	2.1×10^{-7}
4.5029	0.0243	0.0145	2.1×10^{-8}	8.4×10^{-8}	1.3×10^{-7}
5.2360	0.0179	1.1×10^{-9}	1.5×10^{-10}	1.5×10^{-9}	2.5×10^{-9}
5.6549	0.0050	9.4×10^{-12}	8.8×10^{-12}	7.7×10^{-12}	1.4×10^{-11}
6.2413	0.0066	6.1×10^{-13}	6.5×10^{-13}	7.2×10^{-14}	5.4×10^{-14}

compared to Dirichlet mollified solutions. Away from discontinuity, all mollifiers provide similar accuracy. When different P is chosen at different sub-intervals, the accuracy of the mollified solutions has improved significantly at more points near the discontinuities for polynomial mollifiers, which are shown in Figures 2(c) and 2(d) and the Table 4. The following example is an illustration of our mollifier approach on a two dimensional discontinuous function.

Example 3.

$$u(x,y) = \begin{cases} 0.5, \ \pi/2 \le x \le 3\pi/2 \ \& \ \pi/2 \le y \le 3\pi/2 \\ 0, \quad Otherwise. \end{cases}$$

Table 3 Absolute error using Dirichlet, Legendre, Chebyshev kernel mollified solution of Example 2. The discontinuity points are $0, \pi/2, 2\pi$.

Points	Unmollified	Dirichlet [1]	Legendre	Chebyshev
0.0419	0.0773	0.0773	0.0773	0.0773
0.7959	0.0032	0.0032	0.0032	0.0032
1.0472	0.0070	0.0070	0.0070	0.0070
1.5080	0.0502	0.0502	0.0502	0.0502
2.6180	0.0014	0.0014	9.6×10^{-5}	4.4×10^{-5}
3.0997	0.0004	2.0×10^{-5}	1.0×10^{-7}	1.9×10^{-8}
3.3510	0.0022	1.6×10^{-8}	5.2×10^{-9}	1.0×10^{-9}
3.5814	0.0018	6.0×10^{-10}	4.8×10^{-10}	4.7×10^{-10}
3.8746	0.0013	6.5×10^{-12}	2.3×10^{-11}	2.2×10^{-11}
4.1888	0.0045	2.5×10^{-10}	3.5×10^{-10}	5.8×10^{-10}
4.6077	0.0003	2.2×10^{-7}	2.4×10^{-8}	1.1×10^{-8}
4.9218	0.0058	0.0034	3.2×10^{-6}	5.4×10^{-6}
5.4454	0.0052	0.0051	2.9×10^{-6}	1.1×10^{-6}
6.2413	0.0826	0.0826	0.0826	0.0826

Table 4 Absolute error using Dirichlet, adaptive Dirichlet, Legendre, Chebyshev kernel mollified solution of Example 2. The discontinuity points are $0, \pi/2, 2\pi$.

Points	Unmollified	Dirichlet [1]	Adaptive Dirichlet [3]	Legendre (different P)	Chebyshev (different P)
0.0419	0.0773	0.0773	0.4563	0.0773	0.0773
0.7959	0.0032	0.0032	3.7×10^{-6}	8.6×10^{-6}	6.6×10^{-6}
1.0472	0.0070	0.0070	9.5×10^{-7}	0.0027	0.0024
1.5080	0.0502	0.0502	0.2636	0.0502	0.0502
2.6180	0.0014	0.0014	6.9×10^{-8}	5.3×10^{-9}	5.0×10^{-9}
3.0997	0.0004	2.0×10^{-5}	2.6×10^{-10}	3.8×10^{-8}	5.6×10^{-8}
3.3510	0.0022	1.6×10^{-8}	4.4×10^{-12}	5.2×10^{-9}	1.0×10^{-9}
3.5814	0.0018	6.0×10^{-10}	8.0×10^{-11}	4.8×10^{-10}	4.7×10^{-11}
3.8746	0.0013	6.5×10^{-12}	8.4×10^{-12}	2.3×10^{-11}	2.2×10^{-11}
4.1888	0.0045	2.5×10^{-10}	2.7×10^{-11}	3.5×10^{-10}	5.8×10^{-10}
4.6077	0.0003	2.2×10^{-7}	1.8×10^{-10}	3.9×10^{-8}	5.6×10^{-8}
4.9218	0.0058	0.0034	1.7×10^{-8}	3.6×10^{-8}	5.5×10^{-8}
5.4454	0.0052	0.0052	5.3×10^{-8}	2.9×10^{-6}	1.1×10^{-6}
6.2413	0.0826	0.0826	0.0474	0.0826	0.0826

It is clear that $u(x, y)$ is discontinuous on the rectangle $\{(x, y) : x, y = \pi/2 \text{ or } 3\pi/2\}$. This could make mollification more challenging.

Figures 3(a) and 3(b) represent unmollified, and Legendre polynomial mollified Fourier approximations. The unmollified solution exhibits large oscillations, which are subsided in Legendre mollified solution except at the four corners of the rectangle. Figures 4 and Figure 5 present the error plots of the unmollified and mollified (by Legendre, Chebyshev, Dirichlet kernels) Fourier approximation with fixed and adaptive values of P, respectively. While $P = N/4$ is chosen for polynomial mollifiers, $P = N^{0.5}$ is chosen for Dirichlet mollifier (choice different from suggested optimum by Gottlieb and Tadmor [1] in their examples). For Legendre and Chebyshev polynomial mollifiers, $P = N/4$ and $P = N$ are chosen in different sub-domains.

It is visible from the Figures 4(a) - 4(d) that Legendre and Chebyshev mollified solutions are more accurate, except at some $x-$ values along $y = 3.1416$. Comparing Figures 4(b) and 5(b), adaptive P improves the solution marginally. Unlike in earlier

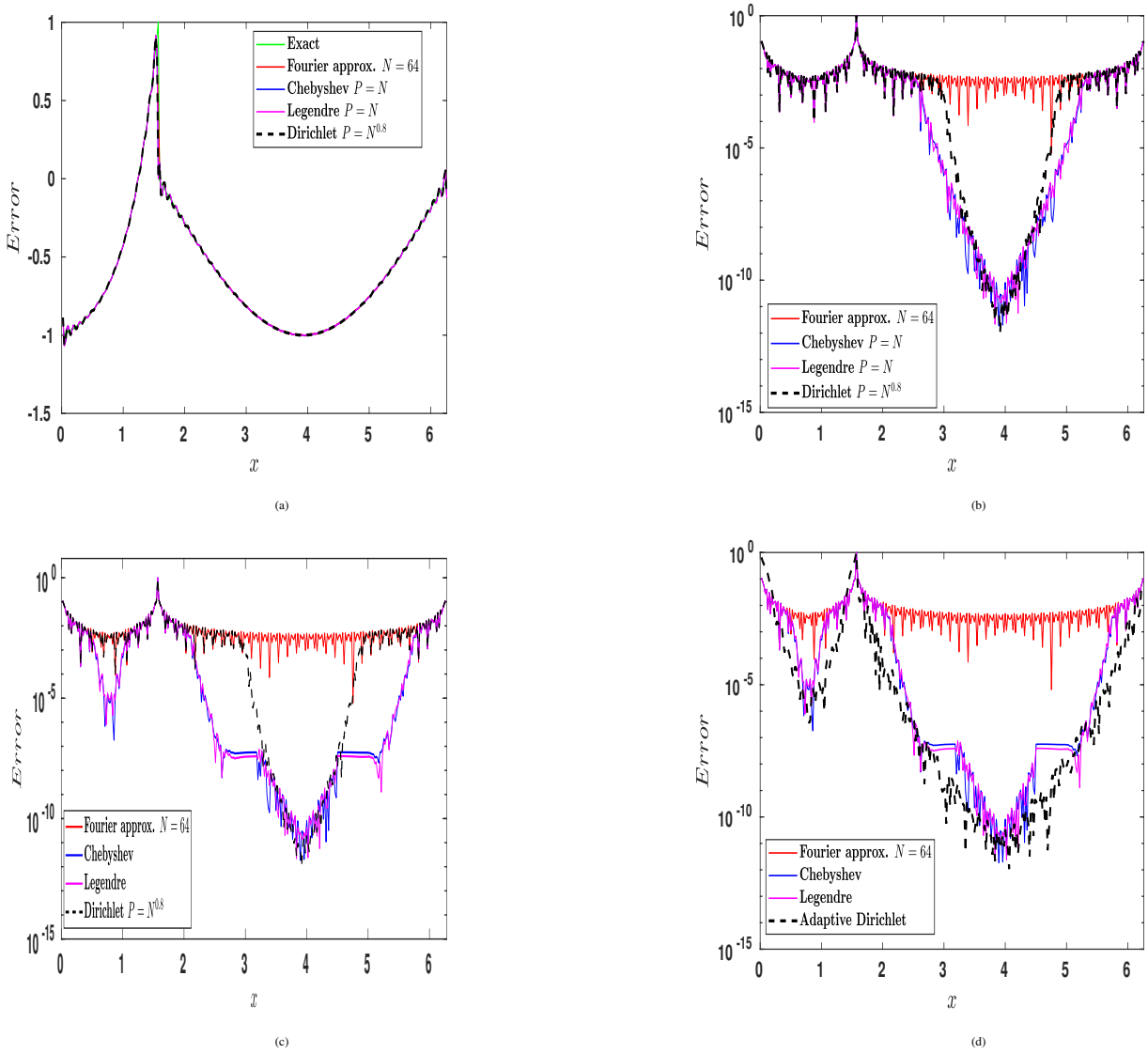

Figure 2 Example 2: Plots of, (a) solution graphs - exact, unmollified and mollified using Legendre, Chebyshev and Dirichlet kernels. (b) Corresponding pointwise error graphs. (c) Legendre and Chebyshev mollification using different P values in different parts of the domain, Dirichlet remain same as in (b), (d) Legendre and Chebyshev mollification is same as in (c), Adaptive Dirichlet mollification by Tadmor and Tanner[3].

examples, considerable improvements in accuracy are not observed with adaptive choice for P over the fixed P. However, along $y = 1.0853$ and $y = 5.6549$, adaptive Dirichlet has shown marginal improvements (see Figures 4(a),4(c) & 5(a), 5(c)).

4.2 | Mollification on Fourier Galerkin approximation of scalar conservation law

In the following we consider one dimensional linear hyperbolic equations with discontinuous initial function.

Example 4.

$$u_t = -2\pi u_x, \quad 0 \le x \le 2\pi, \ t > 0, \quad u(0,t) = u(2\pi,t) \tag{29}$$

$$u(x,0) = \begin{cases} x, & 0 \le x \le \pi \\ x - 2\pi, & \pi < x \le 2\pi. \end{cases}$$

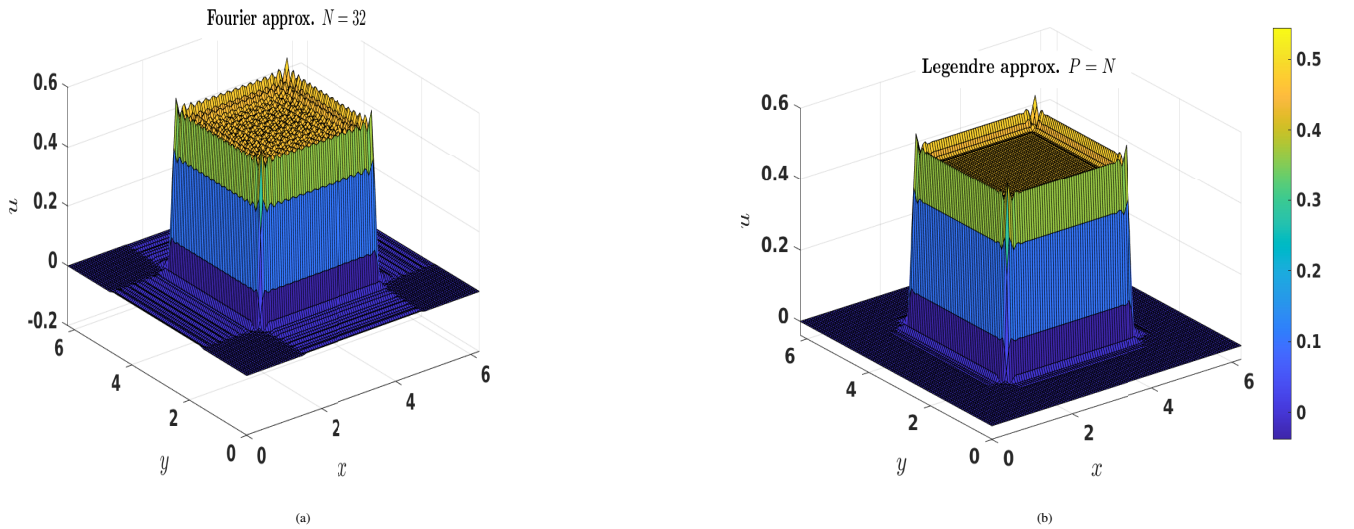

Figure 3 (a) Fourier approximation with $N = 32$. (b) Legendre mollified approximation with $P = N/4$. Chebyshev mollified approximation also shows similar graph.

Example 5.

$$u_t = -2\pi u_x, \quad 0 \le x \le 2\pi, \ t > 0, \quad u(0,t) = u(2\pi,t) \tag{30}$$
$$u(x,0) = \begin{cases} \sin(x/2), & 0 \le x \le \pi, \\ -\sin(x/2), & \pi < x \le 2\pi. \end{cases}$$

In the Fourier Galerkin method, one seeks a solution $S_{\mathcal{N}}u(x,t)$ of the form, $S_{\mathcal{N}}u(x,t) = \sum_{|k|\le N} \hat{u}_k(t)e^{ikx}$, such that the coefficients $\hat{u}_k(t)$ are determined by,

$$\frac{1}{2\pi}\int_0^{2\pi} R_N(x,t)e^{-ikx}dx = 0, \quad \forall\ k = -N, ..., N, \tag{31}$$

where, $R_N(x,t) = \dfrac{\partial\, S_{\mathcal{N}}u(x,t)}{\partial t} + 2\pi\dfrac{\partial\, S_{\mathcal{N}}u(x,t)}{\partial x}$. Substitution of $S_{\mathcal{N}}u(x,t)$ leads to $(2N+1)$ ordinary differential equations (ODEs) to calculate the $(2N+1)$ Fourier coefficients, $\hat{u}_k(t)$ with initial conditions as given below.

$$\frac{d\hat{u}_k(t)}{dt} = -2\pi k\hat{u}_k(t), \quad \forall\ k = -N, ..., N. \tag{32}$$

and

$$\hat{u}_k(0) = \frac{1}{2\pi}\int_0^{2\pi} u(x,0)e^{-ikx}dx, \quad \forall\ k = -N, ..., N.$$

The system of ODEs (32) is solved by the variable separable method. Solution of the above periodic problem (4) is obtained till time $T = 4$. Later, polynomial and Dirichlet mollification is applied to this solution as a post-processing method. Figures of Example 4 show that the methods behave similarly to that in Example 1. Tables 5 and 6 corresponds to Example 4 and Figures 6(a) to 6(d), whereas Tables 7 and 8 corresponds to Example 5. The accuracy of the mollified solution in both fixed P and adaptive P are similar in Example 1. Interestingly, the mollification process recovers accurate solutions at points away from the discontinuity at any time level required without affecting the stability.

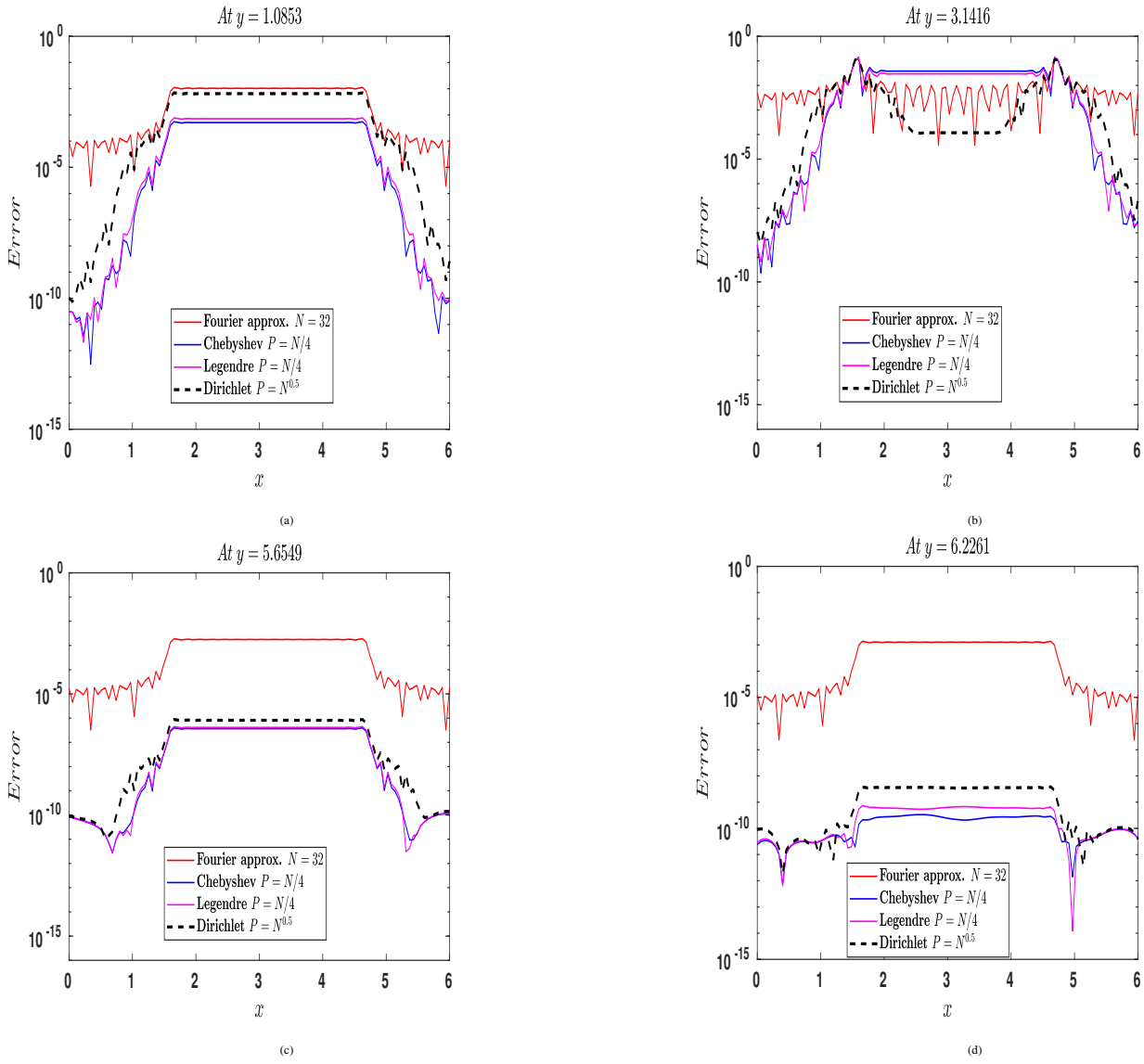

Figure 4 Example 3:-Error plots of, unmollified Fourier approximation with, Dirichlet kernel mollified Fourier approximation ($P = N^{0.5}$), Legendre kernel mollified Fourier approximation ($P = N/4$), Chebyshev kernel mollified Fourier approximation ($P = N/4$) along (a) $y = 1.0853$(b) $y = 3.1416$ (c) $y = 5.6549$ (d) $y = 6.2261$.

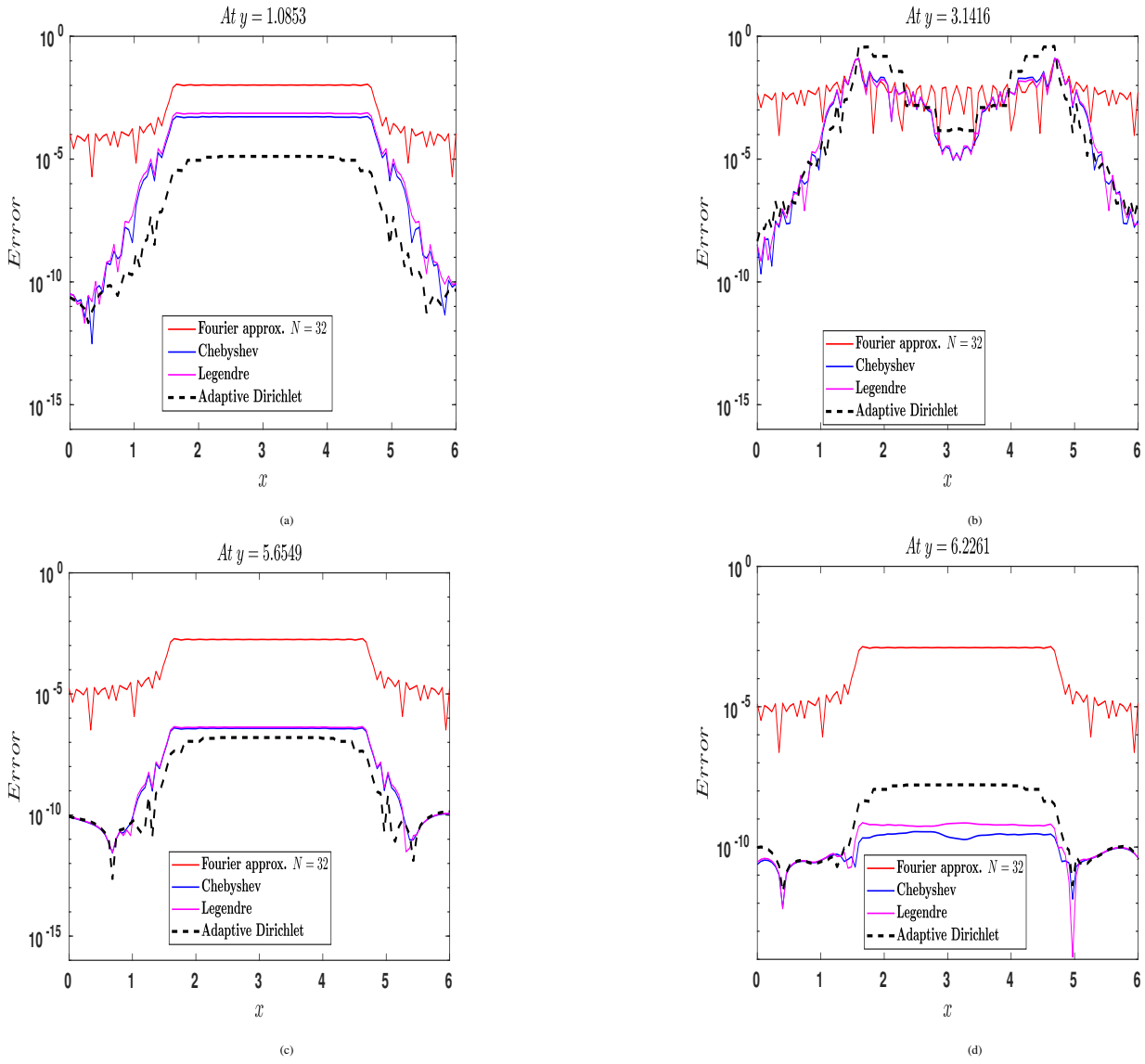

Figure 5 Example 3:-Error plots of, unmollified Fourier approximation with, Dirichlet kernel mollified Fourier approximation ($P = N^{0.5}$), Legendre kernel mollified Fourier approximation, Chebyshev kernel mollified Fourier approximation along (a) $y = 1.0853$(b) $y = 3.1416$ (c) $y = 5.6549$ (d) $y = 6.2261$.

Table 5 Absolute error using Dirichlet, Legendre, Chebyshev kernel mollified solution of Example 4 at time $T = 4$. The discontinuity point is π.

Points	Unmollified	Dirichlet[1]	Legendre	Chebyshev
0.0419	0.0066	3.4×10^{-13}	2.5×10^{-13}	2.7×10^{-13}
0.1047	0.0070	1.2×10^{-12}	4.8×10^{-13}	5.7×10^{-13}
0.2094	0.0126	2.7×10^{-11}	8.6×10^{-13}	6.4×10^{-13}
0.6283	0.0050	9.5×10^{-12}	7.5×10^{-12}	1.4×10^{-11}
1.0472	0.0179	1.1×10^{-9}	1.5×10^{-9}	2.5×10^{-9}
1.9059	0.0109	0.0110	0.00021	0.0001
2.0944	0.0004	0.0004	0.0026	0.0025
2.6180	0.0411	0.0411	0.0411	0.0411
3.1206	0.6992	0.6992	0.6992	0.6992
3.1625	0.6992	0.6992	0.6992	0.6992
4.1888	0.0004	0.0004	0.0026	0.0025
4.5029	0.0243	0.0145	1.8×10^{-5}	2.7×10^{-5}
5.2360	0.0179	1.1×10^{-9}	1.5×10^{-9}	2.5×10^{-9}
5.6549	0.0050	9.1×10^{-12}	7.9×10^{-12}	1.4×10^{-11}
6.2413	0.0066	9.4×10^{-13}	3.2×10^{-13}	3.0×10^{-13}

Table 6 Absolute error using Dirichlet, Legendre, Chebyshev kernel mollified solution of Example 4 at time $T = 4$. The discontinuity point is π.

Points	Unmollified	Dirichlet[1]	Adaptive Dirichlet[3]	Legendre (different P)	Chebyshev (different P)
0.0419	0.0066	3.4×10^{-13}	9.6×10^{-13}	2.5×10^{-13}	2.7×10^{-13}
0.1047	0.0070	1.2×10^{-12}	1.3×10^{-12}	4.8×10^{-13}	5.1×10^{-13}
0.2094	0.0126	2.7×10^{-11}	3.6×10^{-12}	8.6×10^{-13}	6.5×10^{-13}
0.6283	0.0050	9.5×10^{-12}	9.0×10^{-12}	7.5×10^{-12}	1.4×10^{-11}
1.0472	0.0179	3.1×10^{-9}	1.6×10^{-10}	1.4×10^{-9}	2.5×10^{-9}
1.9059	0.0109	0.0110	1.9×10^{-7}	9.8×10^{-8}	1.7×10^{-7}
2.0944	0.0004	0.0004	6.6×10^{-8}	1.8×10^{-7}	2.1×10^{-7}
2.6180	0.0411	0.0412	0.0001	0.0167	0.0148
3.1206	0.6992	0.6992	2.1854	0.6992	0.6992
3.1625	0.6992	0.6992	2.1854	0.6992	0.6992
4.1888	0.0004	0.0004	6.6×10^{-8}	1.8×10^{-7}	2.1×10^{-7}
4.5029	0.0243	0.0145	2.1×10^{-8}	8.4×10^{-8}	1.3×10^{-7}
5.2360	0.0179	1.1×10^{-9}	1.6×10^{-10}	1.5×10^{-9}	2.5×10^{-9}
5.6549	0.0050	9.1×10^{-12}	8.6×10^{-12}	7.9×10^{-12}	1.4×10^{-11}
6.2413	0.0066	9.3×10^{-13}	3.7×10^{-13}	3.2×10^{-13}	3.0×10^{-13}

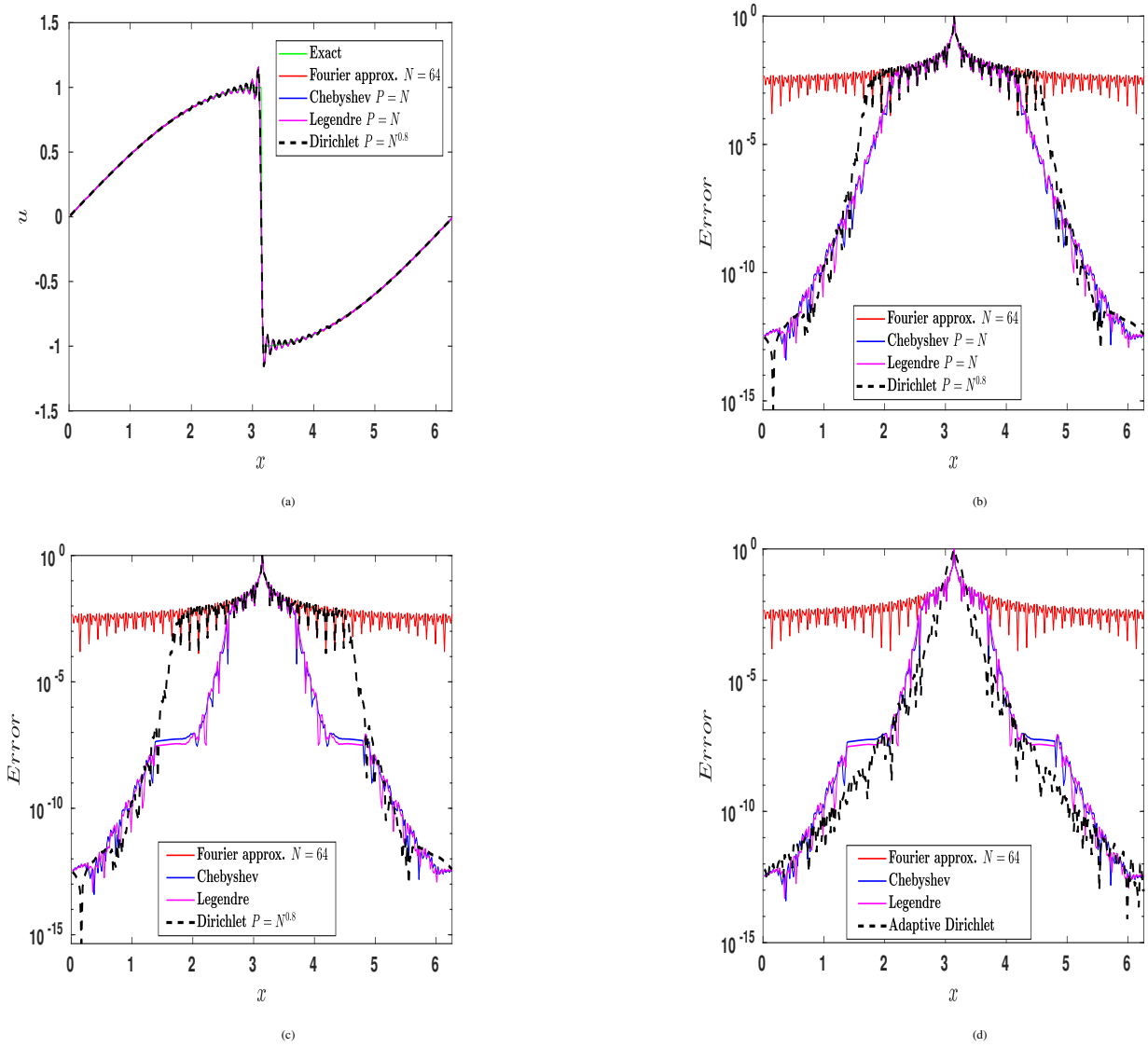

Figure 6 Example 5:- Plots of, (a) solution graphs - exact, unmollified and mollified using Legendre, Chebyshev and Dirichlet kernels at time $T = 4$. (b) Corresponding pointwise error graphs. (c) Legendre and Chebyshev mollification using different P values in different parts of the domain, Dirichlet remain same as in (b), (d) Legendre and Chebyshev mollification is same as in (c), Adaptive Dirichlet mollification by Tadmor and Tanner[3].

Table 7 Absolute error using Dirichlet, Legendre, Chebyshev kernel mollified solution of Example 5 at time $T = 4$. The discontinuity point is π.

Points	Unmollified	Dirichlet[1]	Legendre	Chebyshev
0.0419	0.0021	2.7×10^{-13}	3.4×10^{-13}	3.5×10^{-13}
0.1047	0.0022	1.5×10^{-13}	4.6×10^{-13}	4.7×10^{-13}
0.2094	0.0040	1.5×10^{-13}	6.1×10^{-13}	5.4×10^{-13}
0.6283	0.0016	2.3×10^{-12}	2.7×10^{-12}	4.7×10^{-12}
1.0472	0.00570	3.6×10^{-10}	4.6×10^{-10}	7.9×10^{-10}
1.9059	0.0035	0.0035	6.6×10^{-5}	4.9×10^{-5}
2.0944	0.0001	0.0001	0.0008	0.0008
2.6180	0.0131	0.0131	0.0131	0.0131
3.1206	0.2226	0.2226	0.2226	0.2226
3.1625	0.2226	0.2226	0.2226	0.2226
4.1888	0.0001	0.0001	0.0008	0.0008
4.5029	0.0077	0.00462	5.7×10^{-6}	8.6×10^{-6}
5.2360	0.0057	3.6×10^{-10}	4.6×10^{-10}	7.9×10^{-10}
5.6549	0.0016	2.9×10^{-12}	2.1×10^{-12}	4.1×10^{-12}
6.2413	0.0021	4.4×10^{-13}	3.6×10^{-13}	3.6×10^{-13}

Table 8 Absolute error using Dirichlet, adaptive Dirichlet, Legendre, Chebyshev kernel mollified solution of Example 5 at time $T = 4$. The discontinuity point is π.

Points	Unmollified	Dirichlet[1]	Adaptive Dirichlet[3]	Legendre (different P)	Chebyshev (different P)
0.0419	0.0021	2.7×10^{-13}	5.4×10^{-13}	3.4×10^{-13}	3.5×10^{-13}
0.1047	0.0022	1.5×10^{-13}	7.5×10^{-13}	4.6×10^{-13}	4.7×10^{-13}
0.2094	0.0040	1.5×10^{-13}	8.8×10^{-13}	6.1×10^{-13}	5.4×10^{-13}
0.6283	0.0016	2.3×10^{-12}	2.7×10^{-12}	2.7×10^{-12}	4.7×10^{-12}
1.0472	0.0057	3.6×10^{-10}	5.2×10^{-11}	4.6×10^{-10}	7.9×10^{-10}
1.9059	0.0035	0.0035	6.1×10^{-8}	4.0×10^{-8}	6.6×10^{-8}
2.0944	0.0001	0.0001	1.4×10^{-8}	4.8×10^{-8}	5.3×10^{-12}
2.6180	0.0131	0.0130	3.6×10^{-5}	0.0053	0.0047
3.1206	0.2226	0.2226	0.6997	0.2226	0.2226
3.1625	0.2226	0.2226	0.6997	0.2226	0.2226
4.1888	0.00011	0.0001	1.4×10^{-8}	4.8×10^{-8}	5.3×10^{-12}
4.5029	0.0077	0.00462	5.1×10^{-9}	3.6×10^{-8}	5.5×10^{-8}
5.2360	0.0057	3.6×10^{-10}	5.2×10^{-11}	4.6×10^{-10}	7.9×10^{-10}
5.6549	0.0016	2.9×10^{-12}	3.3×10^{-12}	2.1×10^{-12}	4.1×10^{-12}
6.2413	0.0021	4.4×10^{-13}	1.7×10^{-13}	3.6×10^{-13}	3.6×10^{-13}

5 | CONCLUSION

In the present work, two polynomial mollifiers have been proposed as an alternative to the Dirichlet mollifier for Fourier spectral methods. It is proved that spectral accuracy has been regained for points away from the discontinuity. Numerical results show that Legendre and Chebyshev polynomial mollification methods provide a marginally better solution when compared with the accuracy obtained in Dirichlet mollified solution with trial and error optimum parameter $P = N^{0.8}$ used by Gottlieb and Tadmor[1]. Even for linear advection model problems with discontinuous initial values, a stable approximation could be obtained even at a later time. Further, Legendre and Chebyshev mollifiers were applied using adaptive values of P. i.e., Different choices of P in the sub-interval/region close to discontinuity. This modification has substantially improved the accuracy and reduced the length of the region having Gibbs oscillations around discontinuity. This behavior is analogous to the adaptive Dirichlet mollifier[3]. Hence there is a scope for improving the accuracy by optimizing the parameter P for the proposed polynomial mollifiers. Accurately identifying the discontinuity is essential for problems involving dynamically evolving discontinuities. Therefore combining the mollification approach with suitable edge detection algorithms such as developed by Gelb and co-workers[35] is necessary for equations such as nonlinear conservation laws.

References

1. Gottlieb D, Tadmor E. Recovering pointwise values of discontinuous data within spectral accuracy. In: Springer. ; 1985: 357–375.

2. Abarbanel S, Gottlieb D, Tadmor E. Spectral methods for discontinuous problems. Tech. Rep. ICASE Report No: 85-38, NASA CR-172535; 1985.

3. Tadmor E, Tanner J. Adaptive mollifiers for high resolution recovery of piecewise smooth data from its spectral information. *Found Comput Math* 2002; 2(2): 155–189.

4. Tanner J. Optimal filter and mollifier for piecewise smooth spectral data. *Math Comp* 2006; 75(254): 767–790.

5. Piotrowska J, Miller JM, Schnetter E. Spectral methods in the presence of discontinuities. *J Comput Phys* 2019; 390: 527–547.

6. Gruberger N. Spectral methods for the computation of discontinuous solutions. *J Sci Comput* 1989; 4(1): 71–117.

7. Vandeven H. Family of spectral filters for discontinuous problems. *J Sci Comput* 1991; 6(2): 159–192.

8. Tadmor E, Tanner J. Adaptive filters for piecewise smooth spectral data. *IMA J Numer Anal* 2005; 25(4): 635–647.

9. Yun BI, Rim KS. Construction of Lanczos type filters for the Fourier series approximation. *Appl Numer Math* 2009; 59(2): 280–300.

10. Kanevsky A, Carpenter MH, Hesthaven JS. Idempotent filtering in spectral and spectral element methods. *J Comput Phys* 2006; 220(1): 41–58.

11. Gottlieb D, Shu CW, Solomonoff A, Vandeven H. On the Gibbs phenomenon I: Recovering exponential accuracy from the Fourier partial sum of a nonperiodic analytic function. *J Comput Appl Math*.

12. Gelb A, Tanner J. Robust reprojection methods for the resolution of the Gibbs phenomenon. *Appl Comput Harmon Anal* 2006; 20(1): 3–25.

13. Chen Z, Shu CW. Recovering exponential accuracy in Fourier spectral methods involving piecewise smooth functions with unbounded derivative singularities. *J Sci Comput* 2015; 65(3): 1145–1165.

14. Faghihifar E, Akbari M. Exclusive robustness of Gegenbauer method to truncated convolution errors. *J Comput Phys* 2022; 452: 110911.

15. Shizgal BD, Jung JH. Towards the resolution of the Gibbs phenomena. *J Comput Appl Math* 2003; 161(1): 41–65.

16. Hrycak T, Gröchenig K. Pseudospectral Fourier reconstruction with the modified inverse polynomial reconstruction method. *J Comput Phys* 2010; 229(3): 933–946.

17. Eckhoff KS. Accurate and efficient reconstruction of discontinuous functions from truncated series expansions. *Math Comp* 1993; 61(204): 745–763.

18. Adcock B. Convergence acceleration of modified Fourier series in one or more dimensions. *Math Comp* 2011; 80(273): 225–261.

19. Batenkov D. Complete algebraic reconstruction of piecewise-smooth functions from Fourier data. *Math Comp* 2015; 84(295): 2329–2350.

20. Driscoll TA, Fornberg B. A Padé-based algorithm for overcoming the Gibbs phenomenon. *Numer Algorithms* 2001; 26: 77–92.

21. Min M, Kaber SMO, Don W. Fourier–Padé approximations and filtering for spectral simulations of an incompressible Boussinesq convection problem. *Math Comp* 2007; 76(259): 1275–1290.

22. Hesthaven JS, Kaber SMO, Lurati L. Padé-Legendre interpolants for Gibbs reconstruction. *J Sci Comput* 2006; 28: 337–359.

23. Tadmor E. Convergence of spectral methods for nonlinear conservation laws. *SIAM J Numer Anal* 1989; 26(1): 30–44.

24. Chen GQ, Du Q, Tadmor E. Spectral viscosity approximations to multidimensional scalar conservation laws. *Math Comp* 1993; 61(204): 629–643.

25. Dehghan M, Salehi R. The Chebyshev spectral viscosity method for the time dependent Eikonal equation. *Math Comput Modelling* 2010; 52(1-2): 70–86.

26. Don WS, Gottlieb D. Spectral simulation of supersonic reactive flows. *SIAM J Numer Anal* 1998; 35(6): 2370–2384.

27. Gelb A, Tadmor E. Enhanced spectral viscosity approximations for conservation laws. *Appl Numer Math* 2000; 33(1-4): 3–21.

28. Schwander L, Ray D, Hesthaven JS. Controlling oscillations in spectral methods by local artificial viscosity governed by neural networks. *J Comput Phys* 2021; 431: 110144.

29. Cai W, Gottlieb D, Shu CW. Essentially nonoscillatory spectral Fourier methods for shock wave calculations. *Math Comp* 1989; 52(186): 389–410.

30. Rim KS, Yun BI. Gibbs phenomenon removal by adding Heaviside functions. *Adv Comput Math* 2013; 38: 683–699.

31. Gottlieb D. Spectral methods for compressible flow problems. In: No. ICASE Report No: 84-29. Springer. ; 1984: 48–61.

32. Kaber SMO. Filtering non-periodic functions. *Comput Methods Appl Mech Engrg* 1994; 116(1-4): 123–130.

33. Hesthaven JS, Gottlieb S, Gottlieb D. *Spectral methods for time-dependent problems*. 21. Cambridge University Press . 2007.

34. Canuto C, Hussaini MY, Quarteroni A, Thomas Jr A, others . *Spectral methods in fluid dynamics*. Springer Science & Business Media . 2012.

35. Gelb A, Cates D. Detection of edges in spectral data III—refinement of the concentration method. *J Sci Comput* 2008; 36(1): 1–43.

How to cite this article: Williams K., B. Hoskins, R. Lee, G. Masato, and T. Woollings (2016), A regime analysis of Atlantic winter jet variability applied to evaluate HadGEM3-GC2, *Q.J.R. Meteorol. Soc.*, *2017;00:1–6*.